

# Comparison between non orographic gravity wave parameterizations used in QBOi models and Strateole 2 constant level balloons

F. Lott<sup>1</sup> | R. Rani<sup>1</sup> | C. McLandress<sup>4</sup> | A. Podglajen<sup>1</sup>  
| A. Bushell<sup>5</sup> | M. Bramberger<sup>9</sup> | H.-K. Lee<sup>6</sup> | J.  
Alexander<sup>9</sup> | J. Anstey<sup>4</sup> | H.-Y. Chun<sup>6</sup> | A. Hertzog<sup>2</sup>  
| N. Butchart<sup>5</sup> | Y.-H. Kim<sup>7</sup> | Y. Kawatani<sup>17,18</sup> | B.  
Legras<sup>1</sup> | E. Manzini<sup>8</sup> | H. Naoe<sup>10</sup> | S. Osprey<sup>11</sup> |  
R. Plougonven<sup>3</sup> | H. Pohlmann<sup>8</sup> | J. H. Richter<sup>12</sup> | J.  
Scinocca<sup>4</sup> | J. García-Serrano<sup>13</sup> | F. Serva<sup>14</sup> | T.  
Stockdale<sup>15</sup> | S. Versick<sup>16</sup> | S. Watanabe<sup>18</sup> | K.  
Yoshida<sup>10</sup>

<sup>1</sup>LMD/IPSL, Sorbonne Université, PSL Research Institute, Ecole Normale Supérieure, Paris, France.

<sup>2</sup>LMD/IPSL, Sorbonne Université, Paris, France.

<sup>3</sup>LMD/IPSL, Ecole Polytechnique, Institut Polytechnique de Paris, Palaiseau, France

<sup>4</sup>Canadian Centre for Climate Modelling and Analysis (CCCma), Victoria, Canada

<sup>5</sup>Met Office, FitzRoy Road, Exeter, UK

<sup>6</sup>Yonsei University, Seoul, South Korea

<sup>7</sup>Institut für Atmosphäre und Umwelt, Goethe-Universität, Frankfurt am Main, Germany

<sup>8</sup>Max Planck Institute for Meteorology, Hamburg, Germany

<sup>9</sup>NorthWest Research Associates, Boulder Office, Boulder, CO, USA

<sup>10</sup>Meteorological Research Institute (MRI), Tsukuba, Japan

<sup>11</sup>Atmospheric, Oceanic and Planetary Physics, University of Oxford, Oxford, UK

<sup>12</sup>National Center for Atmospheric Research (NCAR), Boulder, Colorado, USA

<sup>13</sup>Group of Meteorology Universitat de Barcelona, Barcelona, Spain

Gravity Wave (GW) parameterizations from 12 General Circulation Models (GCMs) participating in the Quasi-Biennial Oscillation initiative (QBOi) are compared to Strateole-2 balloon observations made in the tropical lower stratosphere from November 2019 to February 2020 (phase 1) and from October 2021 to January 2022 (phase 2). The parameterizations employ the 3 standard techniques used in GCMs to represent subgrid scale non-orographic GWs, namely the two globally spectral techniques developed by Warner and McIntyre (1999) and Hines (1997), as well as the "multi-waves" approaches following Lindzen (1981). The input meteorological fields necessary to run the parameterizations offline are extracted from the ERA5 reanalysis and corre-

**Correspondence**

Francois Lott, Laboratoire de Météorologie Dynamique, Ecole Normale Supérieure, 24 rue Lhomond, 75231 Paris France  
Email: [francois.lott@sorbonne-universite.fr](mailto:francois.lott@sorbonne-universite.fr)

**Funding information**

FL RR AP MB AH RP: VESRI Schmidt Future project DataWave;  
SW: MEXT program SENTAN, Grant number: JPMXD0722681344

spond to the meteorological conditions found underneath the balloons. In general, there is fair agreement between amplitudes derived from measurements for the waves with periods less than 1 hr and the parameterizations. The correlation between the daily observations and the corresponding results of the parameterization can be around 0.4, which is 99% significant since 1200 days of observations are used. Given that the parameterizations have only been tuned to produce a QBO in the models, the 0.4 correlation coefficient of the GW momentum fluxes is surprisingly good. These correlations nevertheless vary between schemes and depend little on their formulation (globally spectral versus multiwaves for instance). We therefore attribute these correlations to dynamical filtering, which all schemes take into account, whereas only a few relate the gravity waves to their sources. Statistically significant correlations are mostly found for eastward propagating waves, which may be due to the fact that during both Strateole 2 phases the QBO is easterly at the altitude of the balloon flights. We also found that the probability density functions (pdfs) of the momentum fluxes are better represented in spectral schemes with constant sources than in schemes ("spectral" or "multiwaves") that relate GWs only to their convective sources.

**KEYWORDS**

Gravity Waves, Balloon Observations, Quasi-Biennial Oscillation, Global Climate Models

40

**1 | INTRODUCTION**

It is well known that the large scale circulation in the middle atmosphere is in large part driven by gravity waves (GWs) that propagate upward in the stratosphere and mesosphere (Andrews et al., 1987). These waves carry horizontal momentum vertically and interact with the large scale flow when they break. Since the horizontal scale of these waves can be quite short, much shorter than the 1° to 2° horizontal resolution of the atmospheric General Circulation Models (GCMs) used in most Earth System Models they need to be parameterized (Alexander and Dunkerton, 1999). In the tropics, the GWs generated by convection are believed to largely dominate (Fovell et al., 1992; Alexander et al., 2000; Lane and Moncrieff, 2008). These waves also contribute significantly to the forcing of the Quasi-Biennial Oscillation

49 (QBO), a near 28-month oscillation of the zonal mean zonal winds that occurs in the lower part of the equatorial  
50 stratosphere (Baldwin et al., 2001). For these reasons, convectively generated GWs need to be parameterized in  
51 order to simulate a QBO in most GCMs.

52 Although gravity wave parameterizations are now used in many models with success including in the tropics  
53 (Scinocca, 2003; Song and Chun, 2005; Beres et al., 2005; Orr et al., 2010; Lott and Guez, 2013; Bushell et al., 2015;  
54 Anstey et al., 2016; Christiansen et al., 2016; Serva et al., 2018), their validation using direct in situ observations  
55 remains a challenge. Large horizontal-scale GWs can be obtained from global satellite observations of temperature  
56 (Geller et al., 2013) and the corresponding momentum flux computed using polarization relations (Alexander et al.,  
57 2010; Ern et al., 2014). However, in order to observe the shorter horizontal scales that also contribute to the QBO  
58 forcing and to have a direct measurement of the corresponding momentum flux, in situ observations are required. The  
59 most precise measurements are provided by constant-level long-duration balloons, like those made in the Antarctic  
60 region during Strateole-Vorcore (Hertzog, 2007) and Concordiasi (Rabier et al., 2010), or in the deep tropics during  
61 PreConcordiasi (Jewtoukoff et al., 2013) and Strateole 2 (Haase et al., 2018). Among many important results, these bal-  
62 loon observations have shown that the momentum flux entering the stratosphere is extremely intermittent (Hertzog  
63 et al., 2012). This intermittency implies that the mean momentum flux is mostly transported by few large-amplitude  
64 GWs that potentially break at lower altitudes rather than by many uniformly distributed GWs. This intermittent char-  
65 acter, when reproduced by a parameterization (de la Cámara et al., 2014; Kang et al., 2017; Alexander et al., 2021),  
66 can help reduce systematic errors in the midlatitudes, such as the timing of the final warming in the Southern Hemi-  
67 sphere polar stratosphere (de la Cámara et al., 2016), or on the simulation of the QBO (Lott et al., 2012a). Balloon  
68 observations have also been used to characterize the dynamical filtering by the large scale winds (Plougonven et al.,  
69 2017), and to validate the average statistical properties of the GW momentum flux simulated offline using reanalysis  
70 data (Kang et al., 2017; Alexander et al., 2021). For completeness note that here, "dynamical filtering" is the process  
71 by which waves with smaller amplitude intrinsic phase speed break for smaller amplitude MF than the waves with  
72 larger amplitude intrinsic phase speed (see Eq. (3) and the associated discussion in Lott et al. (2023)).

73 However, previous evaluations of parameterizations using balloon observations compared more global statistical  
74 behaviours (Jewtoukoff et al., 2015; Kang et al., 2017; Alexander et al., 2021) rather than ability to reproduce instan-  
75 taneous values of momentum fluxes. One good reason to consider global statistical properties of momentum flux,  
76 rather than daily values, is that parameterizations are based on simplified quasi-linear wave theory, assume spectral  
77 distributions that are loosely constrained, and ignore lateral propagation almost entirely (some attempt to include it  
78 can be found in Amemiya and Sato (2016); Kim et al. (2024), see also the underlying theory in Achatz et al. (2023)).  
79 Nevertheless, some factors could mitigate these weaknesses. One factor is that in all parameterizations the wave  
80 amplitude is systematically limited by a breaking criterion that encapsulates nonlinear effects. Another is that some  
81 parameterizations explicitly relate launched waves to sources, and there is a continuing effort to improve the realism  
82 of the convective sources (Liu et al., 2022). Finally, observations systematically suggest that dynamical filtering by  
83 the large scale wind is extremely important for upward propagating GWs (Plougonven et al., 2017), and this central  
84 property is represented in all GW parameterizations. For all these reasons, it may well be that GW parameterizations  
85 using the large scale flow found at a given place and time produce momentum fluxes that can be directly compared  
86 to those measured by a balloon at the same place.

87 Based on the relative success of previous offline calculations using reanalysis data (Jewtoukoff et al., 2015; Kang  
88 et al., 2017; Alexander et al., 2021), Lott et al. (2023) have shown that such a direct comparison gives results of interest.  
89 The first is that the state-of-the-art convective gravity wave drag scheme of Lott and Guez (2013) predicts momentum  
90 fluxes in the lower equatorial stratosphere whose amplitudes can be directly compared with those measured during  
91 phase 1 of the Strateole-2 balloon campaign. This gives a direct in-situ observational confirmation that the theories

92 and modelling of the QBOs developed over the last 50 years are largely correct about the importance of GWs for  
93 driving the QBO. Moreover, the comparison showed a good level of correlation between the day to day variability in  
94 momentum fluxes between measured and parameterized values, a correlation that is much higher for waves carrying  
95 momentum fluxes in the eastward direction than in the westward direction. Such a good correlation is consistent  
96 with the fact that the Lott and Guez (2013) scheme relates the gravity waves to their convective sources (not all  
97 schemes do) and that the GWs experience strong dynamical filtering in the middle troposphere and lower stratosphere.  
98 However, Lott et al. (2023) also show that a scheme that relates gravity waves to only convection failed to predict the  
99 right statistical behaviour of the momentum fluxes. More precisely, the probability density function of the predicted  
100 momentum flux amplitudes have long tails for low values which are more pronounced than in observations. This  
101 suggests that the parameterization misses processes like lateral propagation or the presence of a background of waves  
102 whose source and nature need to be understood.

103 The purpose of this paper is to extend the direct comparison used in Lott et al. (2023) by including more recent  
104 Strateole 2 observations and different gravity wave parameterizations. Here we use nearly all the parameterizations  
105 used by the modelling groups participating in the Quasi-Biennial Oscillation initiative (QBOi, Butchart et al. (2018)).  
106 We then follow Lott et al. (2023) and use the 8 balloons of the first phase of the Strateole 2 campaign that flew in  
107 the lower tropical stratosphere between November 2019 and February 2020 and add the 15 balloons that flew more  
108 than one day during the second phase of the Strateole 2 campaign, between October 2021 and January 2022. In  
109 those flights and at each time in those flights, we have identified the horizontal grid point in the ERA5 reanalysis  
110 (Hersbach et al., 2020) that is nearest to the balloon location. At those times and places we extract from ERA5 the  
111 vertical profiles of wind and temperature, as well as the surface value of precipitation to calculate the parameterized  
112 GW momentum fluxes. As some parameterizations need them, we also extract from ERA5 analysis and 3hr-forecasts  
113 the diabatic heating rates and the cloud base and cloud top altitudes.

114 The outline of the paper is as follows. Section 2 describes the data and the parameterization schemes used. Sec-  
115 tion 3 compares the MF values calculated with the parameterizations and compare them to the observed values by  
116 evaluating daily correlations, averages over each balloons flight, averages over all the Strateole 2 flights, and distri-  
117 butions (pdfs). Section 4 summarizes the results. As we shall see the performances of each parameterization can be  
118 contrasted regarding that we use one type of result rather than other, but our purpose is not to promote one scheme  
119 in front of the others. Adapting other groups parameterization to a testbed that have been intensively used for LMDz  
120 (see Lott et al. (2023)), can give an unfair advantage to the corresponding scheme, which is absolutely not the objective  
121 of the present work. We return to this point in Section 4.

## 122 | 2 | DATA AND METHOD

### 123 | 2.1 | Parameterizations of non orographic gravity wave schemes

124 The parameterization schemes used in GCMs to calculate non-orographic gravity waves belong to two distinct families,  
125 dating back to the 1980's when it became evident that a simulation of the middle atmosphere by global atmospheric  
126 models could not be done without including subgrid scale GWs.

127 The first family is based on the formulation of Lindzen (1981), where the gravity wave field is represented by  
128 waves that are monochromatic in the horizontal and time. Lindzen's scheme was first extended to treat a large en-  
129 semble of waves by Alexander and Dunkerton (1999) making the assumption that the breaking of each wave could  
130 be made independent from the others. An advantage of such schemes is that they are based on linear theories where  
131 sources like convection and/or fronts can be introduced using closed form solutions (Beres et al., 2005; Song and

	$p_l$	$F_{LT}$	$2\pi/m_*$	$C_{\min}$
CMAM	100hPa	1.3mPa	1km	0.25 m/s
IFS	450hPa	5mPa	3km	0.5 m/s
ECEarth	450hPa	3.75mPa	2km	0.25 m/s
UMGA7gws	1000hPa	$\sqrt{\text{Precip}}$	4.3km	not used

**TABLE 1** WMI Parameters changing between CMAM, IFS, ECEarth, and UMGA7gws. Note that CMAM, IFS, and ECEarth parameterizations are very near each other and described in Scinocca (2003) whereas UMGA7gws follows Warner and McIntyre (1999).

132 Chun, 2005; Richter et al., 2010a; Lott and Guez, 2013; de la Cámara and Lott, 2015; Lott et al., 2012b). In the follow-  
 133 ing we will refer to such schemes as "multiwave". These schemes are expensive because they request a large number  
 134 of harmonics to well represent a realistic wave field, but this limit can easily be circumvented by using stochastic  
 135 approaches (Eckermann, 2011; Lott et al., 2012a).

136 As an alternative, but also to better represent the effect of wave breaking, globally spectral schemes have been  
 137 developed and used with success. These schemes use the observational fact that GWs produce kinetic energy spectra  
 138 which have a quite universal shape when expressed as a function of vertical wavenumber. In the early 1990's Hines  
 139 (1991) developed a theory where GW breaking is represented by imposing an upper limit to the range of vertical  
 140 wavenumbers, the limit being calculated according to the large-scale wind and including a Doppler spreading by the  
 141 other gravity waves (see also Hines, 1997). The scheme has been implemented in various GCMs (see for instance  
 142 Manzini et al., 1997), and will be referred to as "HDS" for "Hines Doppler Spread". As an alternative, the theory in  
 143 Warner and McIntyre (1996) imposes gravity wave saturation according to an empirical spectrum but treat vertical  
 144 changes in the spectrum following the propagation invariant characters of GWs. The theory has been simplified and/or  
 145 optimized to permit implementation, for instance in the UKMO model (Warner and McIntyre, 1999; Scaife et al., 2002)  
 146 and in the CMAM model (Scinocca, 2003), and will be referred henceforth as "WMI" for "Warner and McIntyre". To  
 147 a certain extent, the spectral schemes can also take into account the relation with sources. For instance the HDS  
 148 scheme has been related to fronts in Charron and Manzini (2002), and the UKMO version of the WMI scheme to  
 149 precipitation in Bushell et al. (2015).

150 In the present paper, we compare the GW schemes used in 12 of the models that participate in QBOi, these  
 151 models having horizontal grid resolutions between 50km and 300km, i.e. much too short to resolve explicitly the  
 152 shortest period gravity waves. In these models, the GWs parameterizations all belong to one of the three types of  
 153 schemes described above (WMI, HDS, and Multiwave). Since all the multiwave schemes analysed relate GWs to their  
 154 convective sources and since only one of the spectral scheme does so (i.e., the UMGA7gws WMI scheme in Bushell  
 155 et al. (2015)), the results from spectral scheme in Bushell et al. (2015) will often be presented together with the results  
 156 from the source-related multiwave schemes.

157 Among the 12 models, three (CMAM, IFS and ECEarth) use the Scinocca (2003) version of WMI. The specific  
 158 versions of these schemes used for QBOi are further detailed in Anstey et al. (2016), Orr et al. (2010), and Davini et al.  
 159 (2017) respectively. These schemes essentially differ by four parameters: the launch level pressure  $p_l$ , the launched  
 160 momentum flux  $F_{LT}$ , the characteristic vertical wavenumber  $m_*$  and a minimum intrinsic phase speed in the launched  
 161 spectra, the values of each being given here in Table 1. Note that for EC-Earth the exact value of the parameters in  
 162 Table 1 are from J. García-Serrano (private communication).

163 Five of the 12 models, uses the HDS parameterization discussed in Manzini et al. (1997): ECham5, MIROC, MPIM,

	$p_l$	$\sigma_s$	$2\pi/K^*$	$2\pi/m_{\min}$	$C_{smo}$	$N_{smo}$
ECham5	600hPa	1. $\pm$ 0.2 m/s	125km	0	2	5
MIROC	650hPa	0.95 m/s	250 km	94 km	2	2
MPIM	650hPa	1.2 m/s	125 km	0	2	2
MRI-ESM	700hPa	1.9 m/s	1250 km	190 km	4	2
EMAC	650hPa	1. m/s	125 km	0	2	2

**TABLE 2** HDS Parameters changing between ECham5, MIROC, MPIM, MRI-ESM, and EMAC.

	$p_l$	Phase Speed	$\Delta z$	Source
LMDz	500hPa	Intrinsic=Gauss( 0m/s, 30m/s )	1km	Precip <sup>2</sup>
HadGEM2	850hPa-100hPa	-100m/s<Absolute<100m/s	1km-15km	(Convective Heating) <sup>2</sup>
WACCM	1000hPa-100hPa	-100m/s<Absolute<100m/s	1km-4km	(Convective Heating) <sup>2</sup>

**TABLE 3** Some parameters changing between LMDz, HadGEM2 and WACCM, for information only the schemes being extremely distinct one from the other.

164 MRI-ESM, and EMAC. Their version for QBOi are described in Serva et al. (2018), Watanabe et al. (2011), Pohlmann  
 165 et al. (2013), Naoe and Yoshida (2019), and Jöckel et al. (2010) (see also Roeckner et al. (2006)). They mainly differ by  
 166 three different parameters: the launching level  $p_l$ , the root mean square of the horizontal wind variability due to GWs  
 167 at launch level  $\sigma$ , and the effective horizontal wavenumber  $K^*$  (see Table 2). There are also more numerical parameters  
 168 of secondary importance that differ between models: a minimum value for the cutoff vertical wavenumber  $m_{\min}$ , and  
 169 two parameters that control smoothing in the vertical of the GWs root mean square variance, the coefficient  $C_{smo}$  and  
 170 the number of time the smoothing is applied  $N_{smo}$ . It is important to note that in ECham5 the variability parameter  
 171  $\sigma$  is chosen randomly, with a normal distribution centered at 1m/s with standard deviation 0.2m/s. The usefulness  
 172 of such a stochastic ingredient was initially proposed by Piani et al. (2004) who found that it can help stabilizing the  
 173 QBO variability in large scale models and over decades.

174 Finally the last 4 schemes we consider all link GWs to sources (convection or precipitation). Three are multiwaves  
 175 schemes that have been developed independently from each other: LMDz, HadGEM2, and WACCM. Their versions  
 176 used in QBOi are described in Lott and Guez (2013), Song and Chun (2005), and Richter et al. (2010b). One of these  
 177 schemes uses the ultra simple version of the WMI scheme presented in Bushell et al. (2015) rather than the Scinocca  
 178 (2003)'s version. Note that for both HadGEM2 and WACCM, we do not use the exact version used in the QBOi models  
 179 but rather the offline versions developed by Kang et al. (2017) and Alexander et al. (2021), and which were adapted by  
 180 these authors to interpret observations. Since the differences between the 3 multiwave schemes are too numerous,  
 181 the reader is referred to the above mentioned papers. However, important differences can be outlined in the source  
 182 term, the launching levels and the intrinsic phase speed of the launched waves (for the multiwave schemes see also  
 183 table (3)). More specifically, in LMDz the choice is to relate the launched momentum flux to square precipitation  $P_r^2$   
 184 consistent with linear theory before breaking (Lott and Guez, 2013) whereas in (Bushell et al., 2015) it is related to  
 185  $\sqrt{P_r}$  (see Table 1). Furthermore in LMDz the waves are launched in the mid troposphere whereas in the UMGA7gws  
 186 they are launched in the lower troposphere near the surface. In the HadGEM2 scheme (Song and Chun, 2005; Choi

187 and Chun, 2011), the launched momentum flux is directly related to convective heating distributed in the vertical  
 188 between the cloud bottom and cloud top, the launch altitude being at the cloud top. In this case the launch level can  
 189 vary between 2km and 15km typically and the depth of the heating between 1km and 15km. We will take the same  
 190 inputs used for the HadGEM2 scheme to run the WACCM scheme, using the version in Alexander et al. (2021). Note  
 191 that in WACCM, the heating depth is one quarter of the cloud depth, and ranges between 1km and 4km typically.  
 192 Final important differences are that in LMDz the intrinsic phase speeds are chosen randomly according to a Gaussian  
 193 distribution with 0 mean value and 30m/s standard deviation, whereas in both UMGA7gws and WACCM absolute  
 194 phase speed is used, with values uniformly distributed in the range  $-100\text{m/s} < C_{abs} < 100\text{m/s}$ .

## 195 2.2 | Offline parameterization runs

196 To run the schemes in offline mode we use ERA-5 hourly data of precipitation and 3-hourly winds, surface pressure,  
 197 temperature, cloud liquid and ice water content on a  $1^\circ \times 1^\circ$  horizontal grid to mimic a large-scale climate model of  
 198 fairly high horizontal resolution. Winds, surface pressure, temperature, and water contents are then linearly interpo-  
 199 lated on 1hr interval so that they are synchronised with the precipitation. In the vertical we use data at 67 model  
 200 levels taking every second ERA5 level, again to mimic a typical model's vertical resolution but also to speed up calcu-  
 201 lations. To estimate the vertical profiles of convective heating rates, we follow Fueglistaler et al. (2009) and evaluate  
 202 diabatic heating using ERA5 hourly data from the short range forecasts, computing it as the residual between the  
 203 parameterized temperature tendency and the radiative heating rates (longwave plus shortwave). When needed, we  
 204 also evaluate the cloud bottom and cloud top altitudes using the cloud water content (liquid+ice) given in ERA5.

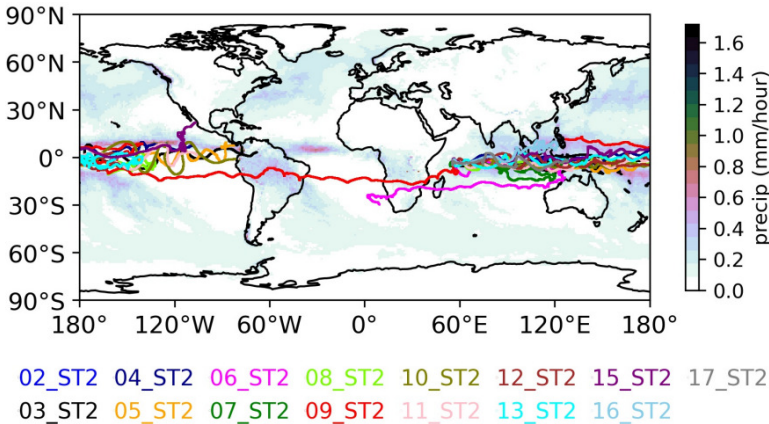


**FIGURE 1** Strateole 2, Phase 2 balloon trajectories taking place between October 2021 and January 2022. Shading presents the precipitation field from ERA5 averaged over the period.

## 205 2.3 | Strateole 2 balloon observations

206 The in situ observations we use are from the 8 balloons of the first phase of the Strateole 2 campaign that flew in the  
 207 tropical lower stratosphere between November 2019 and February 2020 and from the 15 balloons that flew for more

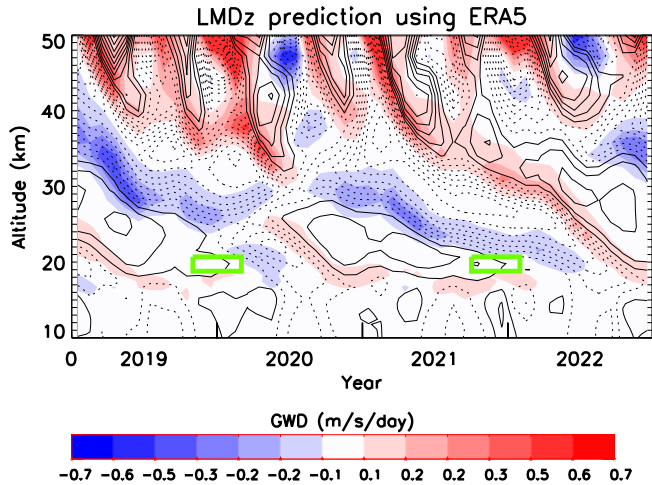


**FIGURE 2** Time vertical sections of the zonal mean zonal wind (CI=10m/s black contours with negative values dashed) and of the non-orographic gravity wave tendency (color shading). All zonal mean fields are averaged over the Equatorial band ( $-6^{\circ}S - +6^{\circ}N$ ). Input data are from ERA5 reanalysis and GWs prediction from the LMDz scheme. The 2 green boxes indicate schematically the altitude and time ranges of the Strateole 2 phase 1 and 2 flights considered in this study.

208 than one day during the second phase of the Strateole 2 campaign, between October 2021 and January 2022. The  
 209 trajectories during phase 2 are shown in Figure 1, superimposed upon which is the averaged precipitation (the same  
 210 Figure but for phase 1 is in Lott et al. (2023)). For the momentum fluxes (MFs) calculated from observations, Corcos  
 211 et al. (2021) distinguish the eastward travelling waves with positive MFs in the zonal direction from the westward  
 212 travelling waves with negative MFs. They also distinguish the waves with short periods (1hr-15mn) from those with  
 213 periods up to one day (1d-15mn). In the following we will follow Lott et al. (2023) and keep the shortest periods,  
 214 because for these periods the momentum flux measured compare well with the GWs momentum fluxes needed in a  
 215 GCM to produce a QBO. This leaves open the issue that waves with longer periods are certainly in the "grey" zone of  
 216 the models and not realistically represented either.

217 To characterize the phase of the QBO during the balloon flights, Fig. 2 shows a time versus altitude cross section  
 218 of the equatorial zonal mean zonal winds and GWD computed in offline mode using the LMDz scheme for 2018-2023  
 219 and averaged over the tropics. The gravity wave drag is negative (positive) where the vertical wind shear is negative  
 220 (positive) consistent with the fact that it contributes to the QBO descent. We also note that the amplitudes vary  
 221 between  $\pm 0.5$  m/s/day, a range characteristic of the parameterized GW drag tendency used in GCMs that produce a  
 222 QBO-like oscillation (Butchart et al., 2018). The figure also indicates with green rectangles the regions and periods  
 223 during which the balloons operated, typically during the end of easterly QBO phase for both phases 1 and 2. As we  
 224 shall see this yields quite comparable results during the two phases, despite the fact that during phase 1 and above  
 225 the altitude the 2nd documented QBO disruption started (Anstey et al., 2021).

226 Our analysis compares the momentum fluxes derived from the balloon data for waves with intrinsic periods below  
 227 1hr and consider the ERA5 data at the points that are the nearest to the balloon. The calculation is then made every  
 228 hour and averaged over the day, partly because it is the time scale needed for some of the schemes to realistically  
 229 sample a GW field, and also because it takes about one day for a balloon flight to cover a model gridscale. Note that



230 some of the sensitivities to these choices are discussed in Lott et al. (2023)'s conclusion.

231 **3 | RESULTS**

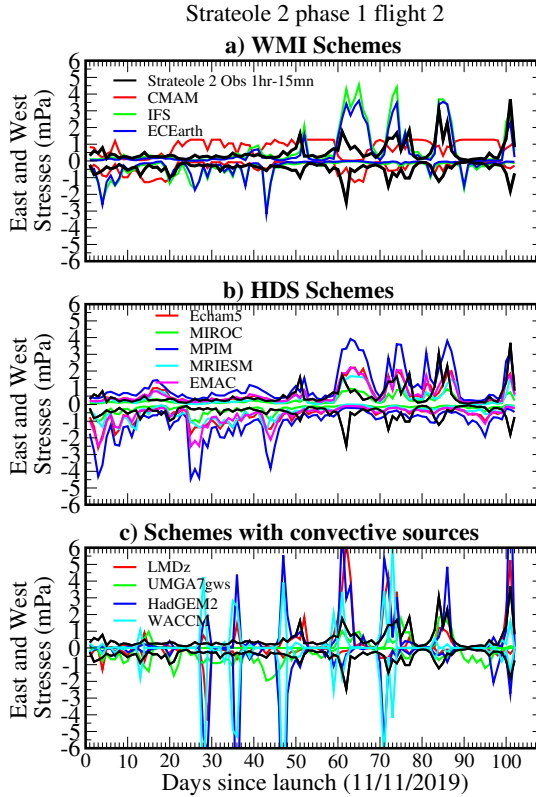


**FIGURE 3** Comparison between daily averaged values of the eastward and westward MFs measured by the balloons during Strateole 2 phase 1 Flight 2 and estimated by the GW schemes at the balloon location and altitude. Colored curves are for the GW schemes using ERA5, black curves are for the observed MFs due to the 15mn-1hr GWs. a) WMI schemes; b) HDS Schemes; c) Schemes relating launched MFs with convective sources or precipitations: all multiwaves except UMGA7gws.

232 Figure 3 shows time series of daily values of momentum fluxes calculated by the parameterizations and measured  
 233 during balloon flight 2 from strateole 2 phase 1. This is also the flight shown in Fig. 3 in Lott et al. (2023), in which  
 234 was shown the time series of daily precipitation and zonal wind at flight altitude. The top panel is for the WMI based  
 235 schemes, the middle panel for the HDS schemes and the bottom panels for the schemes relating the GW fluxes to  
 236 their sources (3 multiwave, 1 WMI). In all panels the black curves are for the daily observations. For clarity we present  
 237 results for the eastward and westward MFs only. Overall one sees that the parameterized MFs somewhat agree  
 238 with the observed ones, at least in term of amplitude. There are nevertheless significant differences in behaviour. For  
 239 instance, the IFS schemes exhibit substantial peaks in eastward flux during the second half of the flight. This is a period

240 during which the zonal wind at flight altitude becomes westward potentially favoring eastward waves consistent with  
 241 dynamical filtering. Note that in Lott et al. (2023) it was shown that the 3 peaks in measured fluxes around days  
 242 60, 75, and 83 also correspond to dates when there was precipitation near the balloon's horizontal location. These  
 243 correspondences made us believe that the relation with convective sources is essential. However, we see here that  
 244 dynamical filtering alone may well be the main cause. Although having smaller amplitudes, the Fig. 3 also shows that  
 245 in EC-Earth, the momentum fluxes behave almost as in IFS. However, the results for CMAM are quite different. In  
 246 this model it was chosen to place the launch altitude near the tropopause. As a consequence the daily time series  
 247 fluctuate less and exhibit long lasting "plateaus". Clearly in this model, the distance between the launch level (100hPa  
 248 see Table 1) and the balloon altitude is too small for dynamical filtering to be efficient. The second panel of Fig. 3  
 249 for the HDS schemes is not fundamentally different from what was discussed above. The amplitude and fluctuations  
 250 are comparable to observed, some schemes predicting values which look either larger or smaller but staying within  
 251 the range of observations. The behaviour of the source related schemes in the third panel of Fig. 3 (multiwave for  
 252 LMDz and HadGEM2, WMI for UMGA7gws) are more contrasted. As expected, there are long periods during which  
 253 the schemes produce small and null momentum fluxes, which are interrupted by short lasting strong peaks. These  
 254 peaks sometime exceed  $\pm 5\text{mPa}$ , which are values never reached by any of the spectral schemes in panels 3a) and 3b).  
 255 In contrast to LMDz and HadGEM2, the UMGA7gws scheme exhibits smaller amplitude MFs and broader peaks. We  
 256 attribute this to the fact that the UMGA7gws scheme relates the launch flux to  $\sqrt{P_r}$  rather than  $P_r^2$  as is done in LMDz,  
 257 or to the square of heating as is done in both HadGEM2 and WACCM.

258 The MF time series for a flight during the second phase of stratoale 2 is shown in Fig. 4. Beyond the fact that the  
 259 flight is shorter than in Fig. 3, a difference in duration that characterizes most of the flights during phase 2 compared  
 260 to phase 1, the overall behaviour stays about the same: the spectral schemes exhibit fluctuations with broader peaks,  
 261 except maybe CMAM, as a result of the higher launch-altitude which results in dynamical filtering not yet being  
 262 efficient at balloon flight altitude. The last panel in Fig. 4 also shows that UMGA7gws exhibits long periods with  
 263 almost no fluxes. For this scheme, the launch height is low in the troposphere (see Table 1) which results in much  
 264 more critical level filtering during the propagation through the troposphere. Finally, in the version of WACCM used  
 265 here, there is one extreme outlier at day 33, with values below  $-10\text{mPa}$ . We only found few of them over the entire  
 266 campaign, and because WACCM has been intentionally tuned to produce from time to time such extreme values in  
 267 MFs.

268 The fact that the different schemes estimate momentum fluxes of about the right amplitude is summarized in  
 269 Fig. 5 where the average of the fluxes over the 18 flights that last more than a month (8 during phase 1, 10 during  
 270 phase 2) are shown. In this figure we see that the predicted values align quite well with the observed ones, though  
 271 some schemes have a tendency to slightly underestimate the fluxes (MIROC, LMDz), and others to overestimate them  
 272 (CMAM, HadGEM2). The WACCM scheme has a quite distinct behaviour, most balloons measure quite lower fluxes  
 273 than parameterized on average, and few much larger ones. On average over all flights these large values average out  
 274 with smaller ones. However, we have to keep in mind that this behaviour is intentional: the version of the WACCM  
 275 scheme we use has been tuned to produce a very intermittent behaviour and sometimes very strong fluxes (Alexander  
 276 et al., 2021). The numbers in each panel are the correlation coefficient between the 18 observed and parameterized  
 277 values of MFs averaged over each flight. They show that the correlations are quite strong in some models, at least in  
 278 the eastward direction. Interestingly some models also have significant medium to high correlations in the westward  
 279 direction (CMAM, LMDz, HadGEM2). This means that parameterizations can capture quite well the low frequency  
 280 variability of the MFs (the changes with period larger than a month). Thus, it is tempting to say that it is good enough  
 281 for the simulation of the QBO.

282 Figure 6 compares the observed and parameterized eastward and westward fluxes averaged over all the balloon

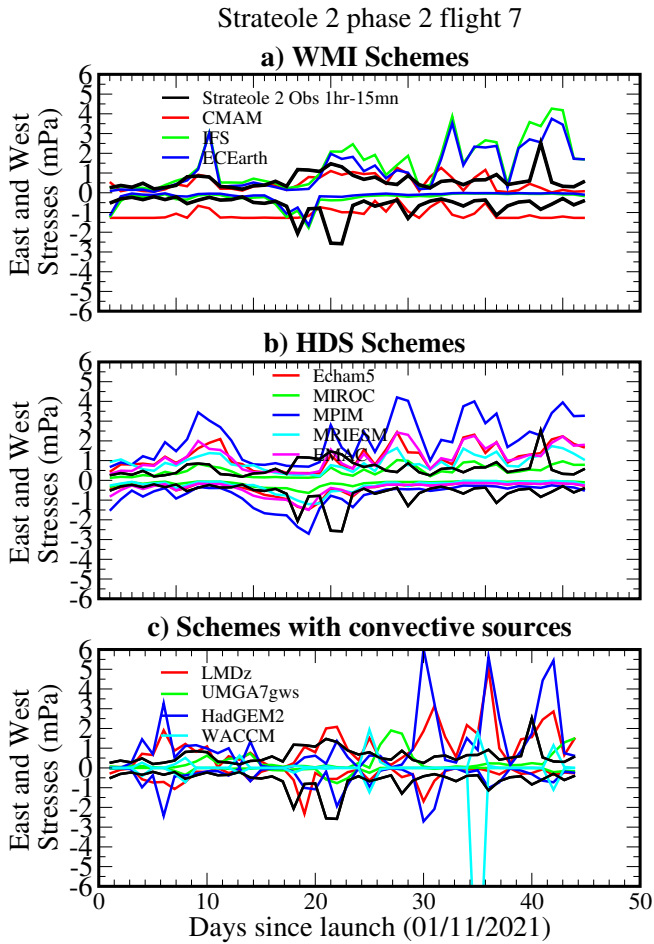


**FIGURE 4** Same as Fig 3 but for Strateole 2 Phase 2 Flight 7.

283 flights, confirming again that the parameterizations fall around the observed values. Although there are differences  
 284 between the models, there is no systematic tendency for them to overestimate or underestimate the observed MF flux  
 285 amplitude. This is elucidated by the green curve which represents the average over all models and over all balloon  
 286 flights. As can be seen the average amplitude of the eastward flux is very near that of the observed (10% overes-  
 287 timate: 0.45mPa for the parameterizations compared to 0.40mPa for the observed), whereas the westward flux is  
 288 overestimated by the models by less than 20% (-0.65mPa for the parameterizations compare to -0.55mPa observed).  
 289 The near 50% error seen in the cumulated flux result from the fact that this flux is the sum of a large positive flux and  
 290 a large amplitude negative flux, the two almost equilibrating each other.

291 The daily time series in Figs 3 and 4 also suggest that observations and offline estimations sometimes evolve  
 292 similarly day after day. A possible reason for this could be that both observed and parameterized MFs are sensitive to  
 293 dynamical filtering, noting that some schemes also take into account convective sources. In the two examples shown  
 294 in Figs. 3 and 4, the correspondence between the observed and parameterized fluxes is quite apparent, particularly

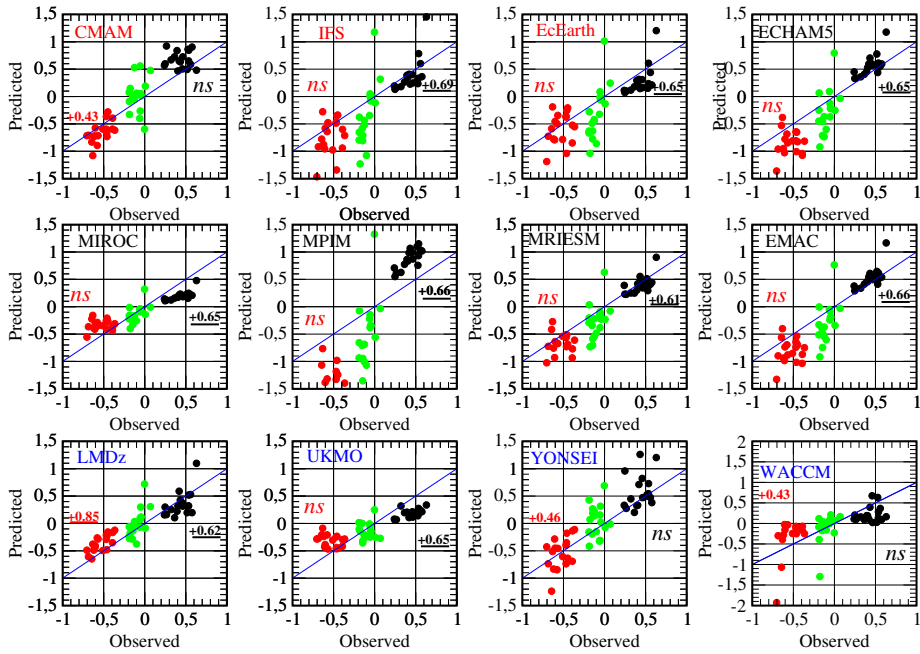


**FIGURE 5** Scatter plot of the momentum fluxes measured by the balloon versus parameterized using different models. Only considered here the 18 balloon flights that last more than a month (East: black; West: red; Cumulated (East+West): green). Also shown are the correlations between observations and predictions, 99% significant levels are bold underlined, 95% are bold. Non significant values indicated by "ns". The number of DoF for Pearson test is 23, which is simply the number of balloon flights and which is therefore very conservative, many balloons lasting more than few weeks, whereas the decorrelation time scale of the daily series being well below a week. Color of the names of the WMI, HDS, and convection-related GWs schemes are in red, black and blue respectively. Note the the change of vertical axis in lower left panel.

295 in the first (Figure 3) in regards to the peaks in the eastward direction discussed earlier. Correspondences are less  
 296 apparent in the second case (Figure 4) where the observed MFs present less variations than the parameterized MFs.  
 297 In Lott et al. (2023) where these daily variations were analysed flight by flight, in some of the flights the time-series  
 298 correlated well whereas in others they did not. This resulted in correlation coefficients  $C$  that are significant but  
 299 "medium" in the eastward direction  $C \approx 0.5$  and "low" to "medium" in the westward direction  $C \approx 0.3$ . Here and in the  
 300 following, we refer to "medium" correlations when  $0.3 < C < 0.5$  and "small" when  $0.1 < C < 0.3$ . As the latter values  
 301 occurred for the LMDz parameterization during Strateole 2 phase 1, the coefficients are given again in the 9th column  
 302 of Table 4. In this table are also given the coefficients for phase 2 and for the phase 1 and 2 combined. Consistent  
 303 with the results found for phase 1, we found during phase 2 medium correlation for the Eastward MF ( $C = 0.4$ ) and  
 304 for the westward MF ( $C = 0.40$ ), the values evaluated over the two phases being medium ( $C = 0.46$  and  $C = 0.34$ ,  
 305 respectively). Here and for completeness, we follow the procedure used in Lott et al. (2023) to test the significance.  
 306 We measure the number of Degrees of Freedom (DoF) for each dataset, and calculate the decorrelation time scale,  
 307 which we take as the lag in day beyond which the lag-autocorrelation of the time-series falls below 0.2. As this time-  
 308 lag varies from one time-series to the other, we give explicitly the DoF in column 2, which is the duration of the flight

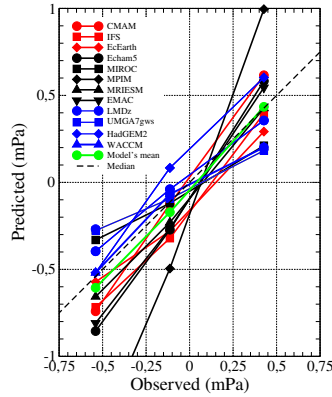


**FIGURE 6** East, West and cumulated zonal momentum fluxes averaged over the Strateole 2 phase 1 and 2 period and according to participating models.

309 divided by the decorrelation time scale. Note that for the decorrelation time, we use for simplicity the daily averaged  
 310 observations, but found that it is not much different from that evaluated with the offline estimates (not shown).

311 When we calculate the daily correlations for the other parameterization schemes, there is also strong variability  
 312 between the flights and the global correlations shown in Table 4 summarize well the averaged behaviour. First, and as  
 313 for LMDz, the correlations evaluated using Phase 2 data stay robust when compared to correlations evaluated using  
 314 phase 1, and whatever is the level of correlation ("medium", "low", or "non significant"). Second, is that many schemes  
 315 managed to have "medium" correlations ( $0.3 < C < 0.5$ ) in the eastward direction. The schemes having no or small  
 316 correlations in the eastward direction (CMAM, HadGEM2, and WACCM) are characterized by the fact that in them  
 317 the launch level is quite high. For instance in CMAM it is near the tropopause which strongly mitigates dynamical  
 318 filtering between the launching level and the balloon altitude. Also interesting, the HadGEM2 and WACCM have low  
 319 or no correlations, in those two models and in the case of deep convection waves are launched from quite high levels  
 320 in the troposphere (not shown) suggesting that in those models as well and for waves with strong eastward flux, there  
 321 is not enough distance between launch levels and balloons altitude for dynamical filtering to be efficient. The results  
 322 in the westward direction are more intriguing. Here the correlations are always small except for one scheme (LMDz)  
 323 and some "low" correlations are found for the two schemes that often launch waves from quite near the tropopause  
 324 (CMAM and HadGEM2). We have difficulties in interpreting this last result. It may mean that launching some waves  
 325 from near the tropopause can improve the westward correlations (as CMAM and HadGEM2 here do), and that always  
 326 launching waves from the same altitude well in the troposphere fails in most cases. But if this is the true, the fact  
 327 that LMDz westward MFs correlate better with observation than any other schemes is in contradiction. Maybe the  
 328 skill of LMDz comes from elsewhere. For instance from the fact that LMDz is a "multiwaves" scheme that explicitly  
 329 launches waves according to their intrinsic frequency, a choice that directly affects dynamical filtering, whereas in the  
 330 globally spectral schemes the dynamical filtering is more indirect and in the other 2 multiwave schemes (HadGEM2  
 331 and WACCM) the waves are launched according to their absolute frequency. These are more speculations given here  
 332 to emphasize the differences that are dynamically significant in our opinion, what is maybe more interesting to notice  
 333 is that there is room to improve GWs parameterizations to obtain better fits between predicted and measured fluxes  
 334 in both directions of propagation, as illustrates the case of LMDz.

335 For this latter model, with moderate intrinsic phase speed range (see Table 3) and therefore strong explicit dynam-

East	Days	CM	IFS	ECE	Ech	MI	MPI	MRI	EM	LMD	UMG	HadG	WAC
	-DoF	AM		ARTH	am5	ROC	M	ESM	AC	z	A7gws	EM2	CM
Phase 1	670-216	ns	<b>0.53</b>	<b>0.52</b>	<b>0.43</b>	<b>0.48</b>	<b>0.49</b>	<b>0.44</b>	<b>0.48</b>	<b>0.49</b>	<b>0.34</b>	<b>0.31</b>	ns
Phase 2	621-322	<b>-0.19</b>	<b>0.41</b>	<b>0.38</b>	<b>0.29</b>	<b>0.33</b>	<b>0.34</b>	<b>0.30</b>	<b>0.33</b>	<b>0.40</b>	<b>0.34</b>	<b>0.20</b>	<b>0.26</b>
1+2	1291-538	-0.11	<b>0.49</b>	<b>0.47</b>	<b>0.35</b>	<b>0.41</b>	<b>0.41</b>	<b>0.36</b>	<b>0.40</b>	<b>0.46</b>	<b>0.34</b>	<b>0.26</b>	ns
West	Days	CM	IFS	ECE	Ech	MI	MPI	MRI	EM	LMD	UMG	HadG	WAC
	-DoF	AM		ARTH	am5	ROC	M	ESM	AC	z	A7gws	EM2	CM
Phase 1	670-216	0.14	ns	ns	ns	ns	ns	ns	ns	<b>0.30</b>	ns	ns	ns
Phase 2	621-322	<b>0.21</b>	<b>0.18</b>	<b>0.16</b>	ns	ns	ns	ns	ns	<b>0.40</b>	ns	0.14	ns
1+2	1291-538	<b>0.17</b>	ns	ns	ns	ns	ns	ns	ns	<b>0.34</b>	ns	0.11	ns

**TABLE 4** Correlation between observed and measured fluxes, strateole phases 1 and 2. 1% significant values according to 2-sided Pearson test are in bold, 5% are in italic, 'ns' stands for non-significant. To evaluate the number of degree of freedom, we proceed as in Lott et al. (2023) and evaluate for each flight the time lag for which the auto correlations of the daily averaged fluxes fall below 0.1 and divide the number of days by that lag.

336 ical filtering, the fact that the westward correlations are significant but lower than the eastward correlations could  
337 follow that the two phase of the campaign are during comparable eastward phase of the QBO, i.e. when eastward  
338 waves are larger in amplitude and more easy to detect (here we assume that waves near saturation have larger ampli-  
339 tude than unsaturated waves and are therefore more easy to detect). It would be instructive to document whether if  
340 westward correlations could be larger when the QBO is westward at the balloon level.

341 As stated in the introduction, more than predicting the right fluxes at the right time, it is often believed that  
342 parameterizations should better be validated against their statistical behaviour. A example is that observed gravity  
343 waves MFs are strongly intermittent, a statistical character that deeply impacts the effect of the waves on the climate  
344 in the middle atmosphere (de la Cámara et al., 2016). In a recent paper, Green et al. (2023) showed that this intermittent  
345 behaviour is well captured when the GWs momentum fluxes have pdfs following a log-normal distribution. These  
346 authors even concluded that in all directions of propagation, momentum flux characteristics could be summarized  
347 in terms of the mean and variance of log normal distributions. As seen in Fig. 7, such lognormal distributions accurately  
348 describe the daily average of the MFs due to the waves with periods between 15mn-1hr deduced from Strateole-2  
349 data. On this figure one sees that the pdfs of the observed fluxes and the log-normal fits are shown in green and blue,  
350 respectively. The fluxes are seen to range in amplitude from 0.1mPa to 10mPa. Furthermore, the pdfs of the westward  
351 fluxes are seen to be shifted toward higher values compared to those for the eastward fluxes, with little change to the  
352 shapes of the curves. The figure also shows that the shifts in the pdfs between eastward and westward fluxes are also  
353 well described by shifts in means and variances of log-normal distributions. For completeness, note nevertheless that  
354 because we use daily averages and also because our dataset is quite short, we miss departures from log-normality  
355 that occurs for the lower values of the MFs documented in Ern et al. (2022).

356 To analyse the QBOi schemes in this framework, Figure 8 presents pdfs of the distributions of the parameterized  
357 daily values of the momentum fluxes. We see that for the WMI schemes (model names in red) the pdfs are much  
358 broader than the observed pdfs (green curves), and often far from log-normal. CMAM and EC-earth for instance  
359 exhibit peaks in the pdfs not located in the middle of the distribution. Quite remarkably, the HDS schemes (model  
360 names in black) are more realistic: the pdfs are narrower and much closer to log normal distributions. It is important  
361 to note that in all the globally spectral schemes without convective sources (WMI and HDS) the shift of the westward  
362 pdfs toward higher values compared to the eastward pdfs is reproduced (except for CMAM). Finally, the schemes

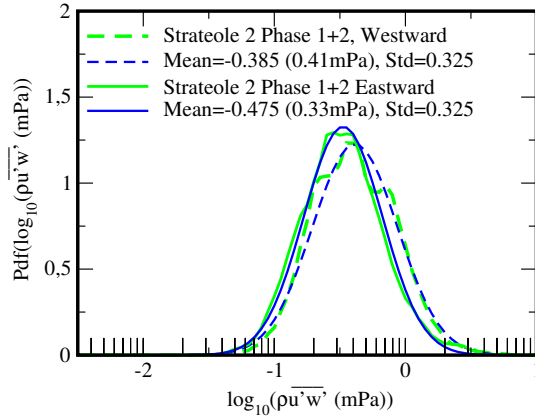


**FIGURE 7** Pdfs of daily values of Momentum flux distribution evaluated from Strateole Phases 1 and 2. The pdfs are calculated from histograms of 1291 MFs daily value within intervals of  $\Delta(\log_{10} \rho u'w' (\text{mPa})) = 0.05$ , thereafter smoothed by a 5 point non-recursive filter with weight (0.1, 0.2, 0.4, 0.2, 0.1). Measured values are in green, log normal fits are in blue. Solid lines are for Eastward, dashed lines are for Westward. Here the log normal probability density function is defined as  $P(X) = \frac{1}{\sqrt{2\pi}\sigma} e^{-\frac{(X-M)^2}{2S^2}}$ , where  $X = \log_{10} \rho |u'w'|$ , and  $M$  and  $S$  the mean and standard deviations given in caption.

363 that relate GWs to convection (names in blue) all have much broader pdfs, with long tails toward small values of the  
 364 MFs. These tails are not realistic which suggests that these parameterizations miss a background of wave activity  
 365 that exists even in the absence of convection nearby. In addition the shift of the westward pdfs toward higher values  
 366 than the eastward pdfs is not apparent. Instead larger westward fluxes eventually occur as a result of changes in pdf  
 367 rather than through translations (see for instance UMG7gws and HadGEM2). If we now return to the conclusions  
 368 of Green et al. (2023) that differences in GW momentum fluxes between directions of propagation could essentially  
 369 be summarized by log-normal pdfs shifted by differences in mean values, one sees that including sources in single  
 370 column parameterizations is not necessarily skilful to achieve this objective. Finally note that the WACCM scheme  
 371 has a larger tail toward higher values (10mPa) than the other schemes, this tail is consistent with the fact that some  
 372 balloons have very large fluxes on average (see Fig. 6).

## 373 4 | CONCLUSION

374 The main result of this paper is that state-of-the-art parameterizations of GWs reproduce reasonably well the eastward  
 375 and westward values of the momentum fluxes due to the high-frequency waves (periods between 15mn and 1hr)  
 376 deduced from in situ measurements made onboard constant-level balloons. In terms of day-to-day variations our  
 377 results are more mitigated: in the eastward direction and without prior tuning many schemes (multiwave HDS or WMI)  
 378 present "medium" correlations with observations; in the westward direction only two schemes produce significant  
 379 ("low" and "medium") correlations. As these results were obtained without any tuning, they suggest that reaching a  
 380 medium level of correlation with daily observations is a possible objective, even in the westward direction. We can  
 381 also found that for our dataset it is easier to find significant correlations for eastward waves than for westward waves,  
 382 this is probably related to the phase of the QBO at the balloons altitudes. It would therefore be important to plan

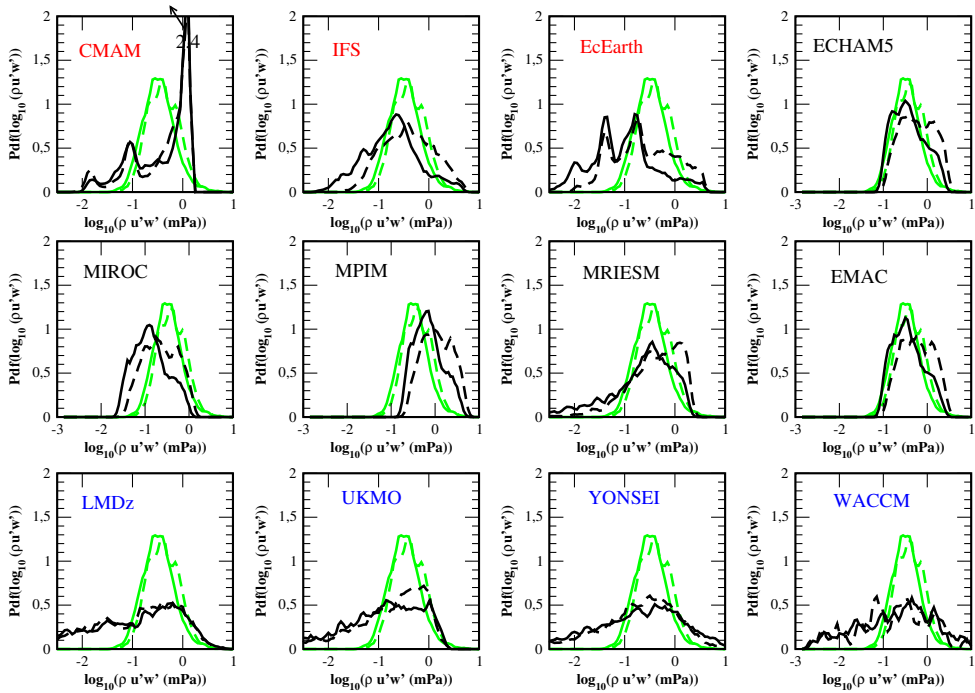


**FIGURE 8** Pdfs of daily values of Momentum flux distribution, same method as in Fig. 7. Measured values are in green, estimations using ERA5 data and the parameterizations are in black. Solid lines are for Eastward, dashed lines are for Westward.

383 another campaign in the opposite phase of the QBO.

384 Due to the low to medium level of the day-to-day correlations we found, we could ask ourselves if it is mandatory  
 385 to improve GW schemes according to such criteria. After all, when the momentum fluxes are averaged over periods  
 386 near a month (here we rather consider averages over balloon flights), the correlations become "medium" to "strong"  
 387 in the eastward direction (see Fig. 5) and sometime medium in the westward direction. Such a level of correlation is  
 388 probably enough in the context of the QBO forcing, since the QBO is evolving over time scales much longer than a  
 389 month.

390 Substantial differences are also found when we compare the pdfs of the parameterized momentum fluxes to  
 391 the pdfs of the measured fluxes. The spectral schemes following the Hines Doppler Spread parameterization (HDS)  
 392 behave the most realistically in this respect. The pdfs for the HDS schemes exhibit one isolated maximum and extend  
 393 broadly along a log normal curve of about the right width. The HDS schemes also reproduce the shift of the pdfs  
 394 toward larger values for the westward MFs, something that the Warner and McIntyre schemes (WMI) also do. The  
 395 fact that both the HDS and WMI spectral schemes reproduce these characteristics is an interesting result. In them  
 396 the source amplitude is constant and they are supposed to represent a broad ensemble of waves, two factors that  
 397 could make them much less intermittent than the multiwave schemes including sources explicitly. It happens that for  
 398 these schemes the dynamical filtering is efficient enough to reproduce a log normal pdf shifted according to the wave  
 399 directions. This is important since log-normal behaviours are significant to the model climate, they capture in good



400 part the intermittency (Green et al., 2023) needed in some models to represent well the final warmings in the southern  
401 hemisphere (de la Cámara et al., 2014) or the fluctuations of the QBO periodicity (Lott and Guez, 2013). As dynamical  
402 filtering is also important to produce log-normal pdfs (Hertzog et al., 2012), it is also not surprising that CMAM fails  
403 in reproducing such a distribution: it launches waves from too near the balloon height for them to be influenced by  
404 the vertical variations in wind during their propagation.

405 The schemes that relate the GWs to convection also have broad momentum flux pdfs, much broader than the  
406 spectral schemes. So in this sense they can be viewed as being even more intermittent than the spectral schemes.  
407 Furthermore they are also characterized by long tails toward small values which seem unrealistic. For these schemes  
408 it therefore seems important to add a background of wave activity even in the absence of convection. This problem  
409 could also be in part corrected out by introducing lateral propagation (Amemiya and Sato, 2016; Kim et al., 2024), a  
410 process that is important in the balloon observations used here (Corcos et al., 2021), but this will not be sufficient  
411 over quite large and dry regions.

412 We did not try to fit the parameters of the schemes we use in order to improve daily correlations or pdfs or both,  
413 but we plan to do it in the near future. We do not have much data though, but could use the Loon data post-processed  
414 in a comparable way as Strateole 2 by Green et al. (2023), which would permit coverage of much wider regions.  
415 We could also complement these observations with the convection permitting global models which outcomes look  
416 promising (Stephan et al., 2016; Köhler et al., 2023; Sun et al., 2023). We should also test if improving the schemes  
417 parameters to improve the fit with observations improves or does not degrade the models climate. It may well be  
418 that parameterizations compensate for potentially resolved equatorial waves for instance, the latter showing a lot of  
419 variability between CMIP5 and QBOi models (Lott et al., 2014; Holt et al., 2022). Also, we could hope that a better fit  
420 with observed values would help reduce persistent systematic errors in the QBO simulations, one of them being that  
421 models underestimate the QBO amplitude in the low stratosphere (Bushell et al., 2022). Unfortunately, our results  
422 are not too promising in this regard: a common believe is that such an error could well be reduced by launching waves  
423 from near the tropopause, but the parameterizations which do so here are not very realistic when it comes to predict  
424 observed MFs variabilities (over days or months).

425 We have also tried to identify if some characteristics or deficiencies in the quasi biennial oscillations simulated in  
426 the QBOi models and reported in the QBOi papers could be related to one or the other characteristics of the schemes  
427 we have analysed. We did not find any, either in terms of periodicities, amplitude, asymmetry as documented in  
428 Bushell et al. (2022), teleconnections with the midlatitudes (Anstey et al., 2022), response to climate change Richter  
429 et al. (2022), equatorial waves amplitude (Holt et al., 2022), and semi annual oscillation (Smith et al., 2022). Of course  
430 in these simulations potential signatures of the parameterizations characteristics can be hidden by the many other  
431 model differences. More thorough test would consist in comparing the different parameterizations online within the  
432 same model. The challenge in this case would be to compare differences once a common target is achieved (for  
433 instance the QBO period and variability at 70hPa).

## 434 Data availability statement

435 All data and routines needed to run the parameterizations in offline mode and to compare the results with the strateole  
436 2 flights are available on a dedicated web site, see details here:

437 <https://web.lmd.jussieu.fr/~flott/DATA/Documentation.pdf>

## references

- 438  
439 Achatz, U., Kim, Y.-H. and Voelker, G. S. (2023) Multi-scale dynamics of the interaction between waves and mean flows: From  
440 nonlinear WKB theory to gravity-wave parameterizations in weather and climate models. *Journal of Mathematical Physics*,  
441 **64**, 111101. URL: <https://doi.org/10.1063/5.0165180>.
- 442 Alexander, M. J., Beres, J. H. and Pfister, L. (2000) Tropical stratospheric gravity wave activity and relationships to clouds.  
443 *Journal of Geophysical Research: Atmospheres*, **105**, 22299–22309.
- 444 Alexander, M. J. and Dunkerton, T. J. (1999) A Spectral Parameterization of Mean-Flow Forcing due to Breaking Gravity Waves.  
445 *J. Atmos. Sci.*, **56**, 4167–4182.
- 446 Alexander, M. J., Geller, M., McLandress, C., Polavarapu, S., Preusse, P., Sassi, F., Sato, K., Eckermann, S., Ern, M., Hertzog, A.,  
447 Kawatani, Y., Pulido, M., Shaw, T. A., Sigmond, M., Vincent, R. and Watanabe, S. (2010) Recent developments in gravity-  
448 wave effects in climate models and the global distribution of gravity-wave momentum flux from observations and models.  
449 *Q. J. R. Meteorol. Soc.*, **136**, 1103–1124.
- 450 Alexander, M. J., Liu, C. C., Bacmeister, J., Bramberger, M., Hertzog, A. and Richter, J. H. (2021) Observational validation of  
451 parameterized gravity waves from tropical convection in the whole atmosphere community climate model. *Journal of*  
452 *Geophysical Research: Atmospheres*, **126**, e2020JD033954.
- 453 Amemiya, A. and Sato, K. (2016) A new gravity wave parameterization including three-dimensional propagation. *Journal of*  
454 *the Meteorological Society of Japan. Ser. II*, **94**, 237–256.
- 455 Andrews, F. G., Holton, J. and Leovy, C. (1987) *Middle Atmosphere Dynamics*. Academic Press.
- 456 Anstey, J. A., Banyard, T. P., Butchart, N., Coy, L., Newman, P. A., Osprey, S. and Wright, C. J. (2021) Prospect of increased  
457 disruption to the QBO in a changing climate. *Geophysical Research Letters*, **48**, e2021GL093058.
- 458 Anstey, J. A., Scinocca, J. F. and Keller, M. (2016) Simulating the qbo in an atmospheric general circulation model: Sensitivity  
459 to resolved and parameterized forcing. *Journal of the Atmospheric Sciences*, **73**, 1649 – 1665.
- 460 Anstey, J. A., Simpson, I. R., Richter, J. H., Naoe, H., Taguchi, M., Serva, F., Gray, L. J., Butchart, N., Hamilton, K., Osprey,  
461 S., Bellprat, O., Braesicke, P., Bushell, A. C., Cagnazzo, C., Chen, C.-C., Chun, H.-Y., Garcia, R. R., Holt, L., Kawatani, Y.,  
462 Kerzenmacher, T., Kim, Y.-H., Lott, F., McLandress, C., Scinocca, J., Stockdale, T. N., Versick, S., Watanabe, S., Yoshida,  
463 K. and Yukimoto, S. (2022) Teleconnections of the quasi-biennial oscillation in a multi-model ensemble of qbo-resolving  
464 models. *Quarterly Journal of the Royal Meteorological Society*, **148**, 1568–1592.
- 465 Baldwin, M. P., Gray, L. J., Dunkerton, T. J., Hamilton, K., Haynes, P. H., Randel, W. J., Holton, J. R., Alexander, M. J., Hirota,  
466 I., Horinouchi, T., Jones, D. B. A., Kinnersley, J. S., Marquardt, C., Sato, K. and Takahashi, M. (2001) The quasi-biennial  
467 oscillation. *Rev. Geophys.*, **39**, 179–229.
- 468 Beres, J. H., Garcia, R. R., Boville, B. A. and Sassi, F. (2005) Implementation of a gravity wave source spectrum parameteriza-  
469 tion dependent on the properties of convection in the whole atmosphere community climate model (waccm). *Journal of*  
470 *Geophysical Research: Atmospheres*, **110**.
- 471 Bushell, A. C., Anstey, J. A., Butchart, N., Kawatani, Y., Osprey, S. M., Richter, J. H., Serva, F., Braesicke, P., Cagnazzo, C., Chen,  
472 C.-C., Chun, H.-Y., Garcia, R. R., Gray, L. J., Hamilton, K., Kerzenmacher, T., Kim, Y.-H., Lott, F., McLandress, C., Naoe,  
473 H., Scinocca, J., Smith, A. K., Stockdale, T. N., Versick, S., Watanabe, S., Yoshida, K. and Yukimoto, S. (2022) Evaluation  
474 of the quasi-biennial oscillation in global climate models for the SPARC-QBO initiative. *Quarterly Journal of the Royal*  
475 *Meteorological Society*, **148**, 1459–1489.
- 476 Bushell, A. C., Butchart, N., Derbyshire, S. H., Jackson, D. R., Shutts, G. J., Vosper, S. B. and Webster, S. (2015) Parameterized  
477 gravity wave momentum fluxes from sources related to convection and large-scale precipitation processes in a global  
478 atmosphere model. *Journal of the Atmospheric Sciences*, **72**, 4349–4371.

- 479 Butchart, N., Anstey, J. A., Hamilton, K., Osprey, S., McLandress, C., Bushell, A. C., Kawatani, Y., Kim, Y.-H., Lott, F., Scinocca, J.,  
480 Stockdale, T. N., Andrews, M., Bellprat, O., Braesicke, P., Cagnazzo, C., Chen, C.-C., Chun, H.-Y., Dobrynin, M., Garcia, R. R.,  
481 Garcia-Serrano, J., Gray, L. J., Holt, L., Kerzenmacher, T., Naoe, H., Pohlmann, H., Richter, J. H., Scaife, A. A., Schenzinger,  
482 V., Serva, F., Versick, S., Watanabe, S., Yoshida, K. and Yukimoto, S. (2018) Overview of experiment design and comparison  
483 of models participating in phase 1 of the sparc quasi-biennial oscillation initiative ("qboi"). *Geoscientific Model Development*,  
484 **11**, 1009–1032.
- 485 Charron, M. and Manzini, E. (2002) Gravity waves from fronts: Parameterization and middle atmosphere response in a general  
486 circulation model. *Journal of the Atmospheric Sciences*, **59**, 923 – 941.
- 487 Choi, H.-J. and Chun, H.-Y. (2011) Momentum flux spectrum of convective gravity waves. part i: An update of a parameteri-  
488 zation using mesoscale simulations. *Journal of the Atmospheric Sciences*, **68**, 739 – 759.
- 489 Christiansen, B., Yang, S. and Madsen, M. S. (2016) Do strong warm enso events control the phase of the stratospheric qbo?  
490 *Geophysical Research Letters*, **43**, 10,489–10,495.
- 491 Corcos, M., Hertzog, A., Plougonven, R. and Podglajen, A. (2021) Observation of gravity waves at the tropical tropopause  
492 using superpressure balloons. *Journal of Geophysical Research: Atmospheres*, **126**, e2021JD035165.
- 493 Davini, P., von Hardenberg, J., Corti, S., Christensen, H. M., Juricke, S., Subramanian, A., Watson, P. A. G., Weisheimer, A. and  
494 Palmer, T. N. (2017) Climate sphinx: evaluating the impact of resolution and stochastic physics parameterisations in the  
495 ec-earth global climate model. *Geoscientific Model Development*, **10**, 1383–1402.
- 496 de la Cámara, A. and Lott, F. (2015) A parameterization of gravity waves emitted by fronts and jets. *Geophys. Res. Lett.*, **42**,  
497 2071–2078.
- 498 de la Cámara, A., Lott, F. and Hertzog, A. (2014) Intermittency in a stochastic parameterization of nonorographic gravity waves.  
499 *J. Geophys. Res.: Atmospheres*, **119**, 11905–11919.
- 500 de la Cámara, A., Lott, F., Jewtoukoff, V., Plougonven, R. and Hertzog, A. (2016) On the gravity wave forcing during the  
501 southern stratospheric final warming in LMDZ. *J. Atmos. Sci.*, **73**, 3213–3226.
- 502 Eckermann, S. D. (2011) Explicitly Stochastic Parameterization of Nonorographic Gravity Wave Drag. *J. Atmos. Sci.*, **68**, 1749–  
503 1765.
- 504 Ern, M., Ploeger, F., Preusse, P., Gille, J., Gray, L. J., Kalisch, S., Mlynczak, M. G., Russell, J. M. and Riese, M. (2014) Interaction  
505 of gravity waves with the QBO: A satellite perspective. *Journal of Geophysical Research: Atmospheres*, **119**, 2329 – 2355.
- 506 Ern, M., Preusse, P. and Riese, M. (2022) Intermittency of gravity wave potential energies and absolute momentum fluxes  
507 derived from infrared limb sounding satellite observations. *Atmospheric Chemistry and Physics*, **22**, 15093–15133.
- 508 Fovell, R., Durran, D. and Holton, J. R. (1992) Numerical simulations of convectively generated stratospheric gravity waves.  
509 *Journal of Atmospheric Sciences*, **49**, 1427 – 1442.
- 510 Fueglistaler, S., Legras, B., Beljaars, A., Morcrette, J.-J., Simmons, A., Tompkins, A. M. and Uppala, S. (2009) The diabatic  
511 heat budget of the upper troposphere and lower/mid stratosphere in ecmwf reanalyses. *Quarterly Journal of the Royal*  
512 *Meteorological Society*, **135**, 21–37.
- 513 Geller, M. A., Alexander, M. J., Love, P. T., Bacmeister, J., Ern, M., Hertzog, A., Manzini, E., Preusse, P., Sato, K., Scaife, A. A.  
514 and Zhou, T. (2013) A comparison between gravity wave momentum fluxes in observations and climate models. *J. Atmos.*  
515 *Sci.*, **26**.
- 516 Green, B., Sheshadri, A., Alexander, M., Bramberger, M. and Lott, F. (2023) Gravity wave momentum fluxes estimated from  
517 project loon balloon data. *Journal of Geophysical Research: Atmospheres*, **Submitted**.
- 518 Haase, J. S., Alexander, M. J., Hertzog, A., Kalnajs, L. E., Deshler, T., Davis, S. M., Plougonven, R., Cocquerez, P. and Venel, S.  
519 (2018) Around the world in 84 days [Dataset]. *Eos*, **99**.

- 520 Hersbach, H., Bell, B., Berrisford, P., Hirahara, S., Horányi, A., Muñoz-Sabater, J., Nicolas, J., Peubey, C., Radu, R., Schepers, D.,  
521 Simmons, A., Soci, C., Abdalla, S., Abellan, X., Balsamo, G., Bechtold, P., Biavati, G., Bidlot, J., Bonavita, M., De Chiara, G.,  
522 Dahlgren, P., Dee, D., Diamantakis, M., Dragani, R., Flemming, J., Forbes, R., Fuentes, M., Geer, A., Haimberger, L., Healy,  
523 S., Hogan, R. J., Hólm, E., Janisková, M., Keeley, S., Laloyaux, P., Lopez, P., Lupu, C., Radnoti, G., de Rosnay, P., Rozum, I.,  
524 Vamborg, F., Villaume, S. and Thépaut, J.-N. (2020) The ERA5 global reanalysis [Dataset]. *Quarterly Journal of the Royal  
525 Meteorological Society*, **146**, 1999–2049.
- 526 Hertzog, A. (2007) The stratéole-vorcore long-duration balloon experiment: A personal perspective. *Space Research Today*,  
527 **169**, 43–48.
- 528 Hertzog, A., Alexander, M. J. and Plougonven, R. (2012) On the Intermittency of Gravity Wave Momentum Flux in the Strato-  
529 sphere. *Journal of the Atmospheric Sciences*, 3433–3448.
- 530 Hines, C. O. (1991) The saturation of gravity waves in the middle atmosphere. part ii: Development of doppler-spread theory.  
531 *Journal of Atmospheric Sciences*, **48**, 1361 – 1379.
- 532 – (1997) Doppler-spread parameterization of gravity-wave momentum deposition in the middle atmosphere. part 2: Broad  
533 and quasi monochromatic spectra, and implementation. *J. Atmos. Solar Terr. Phys.*, **59**, 387–400.
- 534 Holt, L. A., Lott, F., Garcia, R. R., Kiladis, G. N., Cheng, Y.-M., Anstey, J. A., Braesicke, P., Bushell, A. C., Butchart, N., Cagnazzo,  
535 C., Chen, C.-C., Chun, H.-Y., Kawatani, Y., Kerzenmacher, T., Kim, Y.-H., McLandress, C., Naoe, H., Osprey, S., Richter,  
536 J. H., Scaife, A. A., Scinocca, J., Serva, F., Versick, S., Watanabe, S., Yoshida, K. and Yukimoto, S. (2022) An evaluation of  
537 tropical waves and wave forcing of the QBO in the QBOi models. *Quarterly Journal of the Royal Meteorological Society*, **148**,  
538 1541–1567.
- 539 Jewtoukoff, V., Hertzog, A., Plougonven, R., de la Cámara, A. and Lott, F. (2015) Comparison of gravity waves in the southern  
540 hemisphere derived from balloon observations and the ecmwf analyses. *J. Atmos. Sci.*, **72**.
- 541 Jewtoukoff, V., Plougonven, R. and Hertzog, A. (2013) Gravity waves generated by deep tropical convection: Estimates from  
542 balloon observations and mesoscale simulations. *Journal of Geophysical Research: Atmospheres*, **118**, 9690–9707.
- 543 Jöckel, P., Kerkweg, A., Pozzer, A., Sander, R., Tost, H., Riede, H., Baumgaertner, A., Gromov, S. and Kern, B. (2010) Develop-  
544 ment cycle 2 of the modular earth submodel system (messy2). *Geoscientific Model Development*, **3**, 717–752.
- 545 Kang, M.-J., Chun, H.-Y. and Kim, Y.-H. (2017) Momentum flux of convective gravity waves derived from an offline gravity  
546 wave parameterization. part i: Spatiotemporal variations at source level. *Journal of the Atmospheric Sciences*, **74**, 3167 –  
547 3189.
- 548 Kim, Y.-H., Voelker, G. S., Bölöni, G., Zängl, G. and Achatz, U. (2024) Crucial role of obliquely propagating gravity waves in the  
549 quasi-biennial oscillation dynamics. *Atmospheric Chemistry and Physics*, **24**, 3297–3308.
- 550 Köhler, L., Green, B. and Stephan, C. C. (2023) Comparing loon superpressure balloon observations of gravity waves in the  
551 tropics with global storm-resolving models. *Journal of Geophysical Research: Atmospheres*, **128**.
- 552 Lane, T. P. and Moncrieff, M. W. (2008) Stratospheric gravity waves generated by multiscale tropical convection. *J. Atmos. Sci.*,  
553 **65**, 2598–2614.
- 554 Lindzen, R. S. (1981) Turbulence and stress owing to gravity wave and tidal breakdown. *J. Geophys. Res.*, **86**, 9707–9714.
- 555 Liu, C., Alexander, J., Richter, J. and Bacmeister, J. (2022) Using trmm latent heat as a source to estimate convection  
556 induced gravity wave momentum flux in the lower stratosphere. *Journal of Geophysical Research: Atmospheres*, **127**,  
557 e2021JD035785. E2021JD035785 2021JD035785.
- 558 Lott, F., Denvil, S., Butchart, N., Cagnazzo, C., Giorgetta, M. A., Hardiman, S. C., Manzini, E., Krismer, T., Duvel, J.-P., Maury, P.,  
559 Scinocca, J. F., Watanabe, S. and Yukimoto, S. (2014) Kelvin and rossby-gravity wave packets in the lower stratosphere of  
560 some high-top cmip5 models. *Journal of Geophysical Research: Atmospheres*, **119**, 2156–2173.

- 561 Lott, F. and Guez, L. (2013) A stochastic parameterization of the gravity waves due to convection and its impact on the  
562 equatorial stratosphere. *J. Geophys. Res.*, **118**, 8897–8909.
- 563 Lott, F., Guez, L. and Maury, P. (2012a) A stochastic parameterization of non-orographic gravity waves: Formalism and impact  
564 on the equatorial stratosphere. *Geophys. Res. Lett.*, **39**, L06807.
- 565 Lott, F., Plougonven, R. and Vanneste, J. (2012b) Gravity waves generated by sheared three-dimensional potential vorticity  
566 anomalies. *Journal of the Atmospheric Sciences*, **69**, 2134–2151.
- 567 Lott, F., Rani, R., Podglajen, A., Codron, F., Guez, L., Hertzog, A. and Plougonven, R. (2023) Direct comparison between a  
568 non-orographic gravity wave drag scheme and constant level balloons. *Journal of Geophysical Research: Atmospheres*, **128**,  
569 e2022JD037585.
- 570 Manzini, E., McFarlane, N. A. and McLandress, C. (1997) Impact of the doppler spread parameterization on the simulation  
571 of the middle atmosphere circulation using the ma/echam4 general circulation model. *Journal of Geophysical Research:*  
572 *Atmospheres*, **102**, 25751–25762.
- 573 Naoe, H. and Yoshida, K. (2019) Influence of quasi-biennial oscillation on the boreal winter extratropical stratosphere in qboi  
574 experiments. *Quarterly Journal of the Royal Meteorological Society*, **145**, 2755–2771.
- 575 Orr, A., Bechtold, P., Scinocca, J., Ern, M. and Janiskova, M. (2010) Improved middle atmosphere climate and forecasts in the  
576 ecmwf model through a nonorographic gravity wave drag parameterization. *Journal of Climate*, **23**, 5905 – 5926.
- 577 Piani, C., Norton, W. A. and Stainforth, D. A. (2004) Equatorial stratospheric response to variations in deterministic and stochas-  
578 tic gravity wave parameterizations. *Journal of Geophysical Research: Atmospheres*, **109**.
- 579 Plougonven, R., Jewtoukoff, V., de la Cámara, A., Lott, F. and Hertzog, A. (2017) On the relation between gravity waves and  
580 wind speed in the lower stratosphere over the southern ocean. *J. Atmos. Sci.*, **74**, 1075–1093.
- 581 Pohlmann, H., Müller, W. A., Kulkarni, K., Kameswarrao, M., Matei, D., Vamborg, F. S. E., Kadow, C., Illing, S. and Marotzke, J.  
582 (2013) Improved forecast skill in the tropics in the new miklip decadal climate predictions. *Geophysical Research Letters*,  
583 **40**, 5798–5802.
- 584 Rabier, F., Bouchard, A., Brun, E., Doerenbecher, A., Guedj, S., Guidard, V., Karbou, F., Peuch, V., El Amraoui, L., Puech, D.,  
585 Genthon, C., Picard, G., Town, M., Hertzog, A., Vial, F., Cocquerez, P., Cohn, S. A., Hock, T., Fox, J., Cole, H., Parsons, D.,  
586 Powers, J., Romberg, K., Vanandel, J., Deshler, T., Mercer, J., Haase, J. S., Avallone, L., Kalnajs, L., Mechoso, C. R., Tangborn,  
587 A., Pellegrini, A., Frenot, y., Thépaut, J.-N., McNally, A., Balsamo, G. and Steinle, P. (2010) The Concordiasi Project in  
588 Antarctica. *Bulletin of the American Meteorological Society*, **91**, 69–86.
- 589 Richter, J. H., Butchart, N., Kawatani, Y., Bushell, A. C., Holt, L., Serva, F., Anstey, J., Simpson, I. R., Osprey, S., Hamilton, K.,  
590 Braesicke, P., Cagnazzo, C., Chen, C.-C., Garcia, R. R., Gray, L. J., Kerzenmacher, T., Lott, F., McLandress, C., Naoe, H.,  
591 Scinocca, J., Stockdale, T. N., Versick, S., Watanabe, S., Yoshida, K. and Yukimoto, S. (2022) Response of the quasi-biennial  
592 oscillation to a warming climate in global climate models. *Quarterly Journal of the Royal Meteorological Society*, **148**, 1490–  
593 1518.
- 594 Richter, J. H., Sassi, F. and Garcia, R. R. (2010a) Toward a physically based gravity wave source parameterization in a general  
595 circulation model. *Journal of the Atmospheric Sciences*, **67**, 136 – 156.
- 596 – (2010b) Toward a Physically Based Gravity Wave Source Parameterization in a General Circulation Model. *J. Atmos. Sci.*, **67**,  
597 136–156.
- 598 Roeckner, E., Brokopf, R., Esch, M., Giorgetta, M., Hagemann, S., Kornblueh, L., Manzini, E., Schlese, U. and Schulzweida, U.  
599 (2006) Sensitivity of simulated climate to horizontal and vertical resolution in the echam5 atmosphere model. *Journal of*  
600 *Climate*, **19**, 3771 – 3791.
- 601 Scaife, A. A., Butchart, N., Warner, C. D. and Swinbank, R. (2002) Impact of a spectral gravity wave parameterization on the  
602 stratosphere in the met office unified model. *Journal of the Atmospheric Sciences*, **59**, 1473 – 1489.

- 603 Scinocca, J. F. (2003) An accurate spectral nonorographic gravity wave drag parameterization for general circulation models.  
604 *Journal of the Atmospheric Sciences*, **60**, 667 – 682.
- 605 Serva, F., Cagnazzo, C., Riccio, A. and Manzini, E. (2018) Impact of a stochastic nonorographic gravity wave parameterization  
606 on the stratospheric dynamics of a general circulation model. *Journal of Advances in Modeling Earth Systems*, **10**, 2147–  
607 2162.
- 608 Smith, A. K., Holt, L. A., Garcia, R. R., Anstey, J. A., Serva, F., Butchart, N., Osprey, S., Bushell, A. C., Kawatani, Y., Kim, Y.-H.,  
609 Lott, F., Braesicke, P., Cagnazzo, C., Chen, C.-C., Chun, H.-Y., Gray, L., Kerzenmacher, T., Naoe, H., Richter, J., Versick, S.,  
610 Schenzinger, V., Watanabe, S. and Yoshida, K. (2022) The equatorial stratospheric semiannual oscillation and time-mean  
611 winds in qboi models. *Quarterly Journal of the Royal Meteorological Society*, **148**, 1593–1609.
- 612 Song, I.-S. and Chun, H.-Y. (2005) Momentum flux spectrum of convectively forced internal gravity waves and its application  
613 to gravity wave drag parameterization. part i: Theory. *J. Atmos. Sci.*, **62**, 107–124.
- 614 Stephan, C., Alexander, M. J. and Richter, J. H. (2016) Characteristics of gravity waves from convection and implications for  
615 their parameterization in global circulation models. *J. Atmos. Sci.*, **73**, 2729–2742.
- 616 Sun, Y. Q., Hassanzadeh, P., Alexander, M. J. and Kruse, C. G. (2023) Quantifying 3d gravity wave drag in a library of tropical  
617 convection-permitting simulations for data-driven parameterizations. *Journal of Advances in Modeling Earth Systems*, **15**,  
618 e2022MS003585.
- 619 Warner, C. D. and McIntyre, M. E. (1996) On the propagation and dissipation of gravity wave spectra through a realistic middle  
620 atmosphere. *J. Atmos. Sci.*, **53**, 3213–3235.
- 621 – (1999) Toward an ultra-simple spectral gravity wave parameterization for general circulation models. *Earth, Planets and*  
622 *Space*, **51**, 475–484.
- 623 Watanabe, S., Hajima, T., Sudo, K., Nagashima, T., Takemura, T., Okajima, H., Nozawa, T., Kawase, H., Abe, M., Yokohata, T., Ise,  
624 T., Sato, H., Kato, E., Takata, K., Emori, S. and Kawamiya, M. (2011) Miroc-esm 2010: model description and basic results  
625 of cmip5-20c3m experiments. *Geoscientific Model Development*, **4**, 845–872.